Fuel 319 (2022) 123727

Contents lists available at ScienceDirect

Fuel

journal homepage: www.elsevier.com/locate/fuel

Design of Co-Sn bimetallic nanoalloys as electrocatalyst for alkaline methanol oxidation reaction: Exploring the effect of electroactivation process

Zeynab Dabirifar [a], Sara Khadempir [a,*], Alireza Kardan [a], Ceren Karaman [b,*], Onur Karaman [c], Mehmet Lütfi Yola [d]

[a] Department of Chemical Engineering and Energy, Quchan University of Technology, Quchan 9477177870, Iran
[b] Department of Electricity and Energy, Akdeniz University, Antalya 07070, Turkey
[c] Department of Medical Imaging Techniques, Akdeniz University, Antalya 07070, Turkey
[d] Hasan Kalyoncu University, Faculty of Health Sciences, Department of Nutrition and Dietetics, Gaziantep, Turkey

ARTICLE INFO

Keywords:
Electrocatalyst
Direct Methanol Fuel Cell
Bimetallic alloys
Co-Sn Nanoparticles
Artificial neural networks

ABSTRACT

The engineering of cost-effective and durable electrocatalysts for the methanol oxidation reaction (MOR) is required for the commercialization of direct methanol fuel cells (DMFCs). Herein, a series of Co_x-Sn_{100-x} alloy nanoparticles were synthesized to optimize the Co/S ratio, and the alloy nanoparticle which offered the best electrochemical performance towards MOR was employed as electrocatalyst for further experiments. Moreover, two different electroactivation approaches including i) activation in phosphate buffer medium, and ii) *in-situ* activation were explored to enlighten their effect on electrochemical characteristics of nanocatalyst. In this regard, the chronoamperometry measurements were carried out at a constant potential over a fixed period of 300 s. Additionally, the pH of the phosphate buffer solution in a range of 3–12, the activation potential ranging −0.7 V to −2.0 V were optimized by evaluating the recorded cyclic voltammograms. Moreover, to predict the effect of phosphate buffer pH in the activation process on the electrocatalytic activity of catalyst were artificial neural network (ANN) approach was implemented. Amongst the various nanoalloys, Co_{65}-Sn_{35} nanoparticles were determined as the optimal one thanks to their uniform dispersion and less aggregation feature. In the activation process with phosphate buffer at pH of 10 was determined as the optimal, and at this condition a hydrogen evolution reaction also occurred in the range of applied activation potential. The findings revealed that activation in phosphate buffer solution led to the formation of more –OH species, thereby boosting the electrocatalytic activation towards MOR in alkaline media. Similarly, for the *in-situ* activation approach, the optimum potential was determined as −1.3 V to achieve the maximum current density. The findings offered that the electroactivation in phosphate buffer solution (pH = 10) at −1.3 V could result in a highly active electrocatalyst to be utilized in alkaline DMFCs. This research lays the door for tailoring high-performance, low-cost electrocatalysts that could be used in energy conversion systems instead of commercial noble-metal-based electrocatalysts.

1. Introduction

The gradual rise in population and advancements in industrialization have resulted in a greater demand for solutions to increased energy demand and efficient management [1–3]. In this regard, the engineering of efficient high-performance energy storage and conversion systems has gained critical importance, as well as the utilization of sustainable energy sources [4–7]. Amongst the various energy storage and conversion systems, direct alcohol fuel cells have been regarded as the most viable alternatives thanks to their outstanding features including high power densities, wide operating temperature ranges, environmentally friendly nature, storage, and transportation safety [8,9]. Thanks to the advantages of methanol fuel, direct methanol fuel cells (DMFCs) are the greatest situated for widespread commercialization among the diverse cell configurations and fuel types [10,11]. Methanol has numerous benefits including proper storage and transportation, widespread

* Corresponding authors.
E-mail addresses: s.khadempir@qiet.ac.ir (S. Khadempir), cerenkaraman@akdeniz.edu.tr (C. Karaman).

https://doi.org/10.1016/j.fuel.2022.123727
Received 11 January 2022; Received in revised form 17 February 2022; Accepted 26 February 2022
Available online 4 March 2022

availability, low emissions, and potential production from biomasses, besides its high power and energy density values [12]. However, the primary obstacle in the practical commercialization of the DMFCs is the high cost of cells, in which the highest part is the noble metal-based catalyst cost [13]. Moreover, another challenge is the engineering of low-cost high-performance electrocatalysts with long-term stability and high tolerance to toxic intermediates [14]. Thanks to the state-of-art developments in nanotechnology specifically synthesis of multifunctional nanomaterials such as metal-based nanocomposites [15–18], hydrogels/aerogels and their composites [19,20], carbonaceous materials , polymers and their composites [21,22] have been garnered substantial attention thanks to their possible utilization in various application areas such as biomedical [23], environmental applications [24–28], energy [29,30] , sensors [31–34] as well as catalyst [35–37], etc. Hence, benefiting from the advantages of the recent developments in nanomaterial science, it is of great importance to tailor and design noble-metal free electrocatalysts to be utilized in low-cost high-performance DMFCs [38]. Among various alternative electrocatalysts, tin-based alloys (M_xSn_y: M = Co, Ni, Sb, Ag, Cu, Fe, etc.) have been getting attention to be employed as electrocatalysts in energy storage and conversion systems, owing to their outstanding electrochemical features [39–41]. According to reported studies, Sn-based alloys facilitate the decomposition of H_2O on its surface, resulting in increased CO oxidation into CO_2, thereby enhancing tolerance to the poisoning by toxic intermediate species [42]. Among the other possible alternatives, cobalt, a relatively abundant metal in the earth's crust, has been widely preferred in electrochemical energy storage and conversion systems as either the anode material or electrocatalyst [43]. On the other hand, surprisingly, to the best of the authors' knowledge the electrochemical performance of CoSn alloy derivatives has yet to be examined as an electrocatalyst in alkaline DMFCs.

Bearing all in mind, it was aimed to synthesize CoSn alloy nanoparticles and to investigate their potential utilization as electrocatalyst in alkaline direct methanol fuel cells. In this regard, various CoSn alloy nanoparticles were synthesized with different Co/Sn ratios to optimize the catalyst. Moreover, considering the role of metal oxides for boosting electrocatalytic performance and facilitating the removal of adsorbed carbon monoxide species on the catalyst surface by providing adsorbed hydroxyl intermediates, electrochemical *in-situ* transformation of metal atoms to metal oxides was conducted by applying different limit potentials during cyclic voltammetry experiments. Additionally, two different electrochemical activation processes including activation in phosphate buffer solution with different pH values and *in-situ* electrochemical application were carried out by chronoamperometry technique to boost the electrocatalytic activity of the electrocatalyst. The effects of applied potential during the activation process and also pH of the phosphate buffer solution onto the electrochemical behavior of the electrocatalyst were investigated, and at the same time, the potential for hydrogen evolution reaction was evaluated at optimized conditions. Furthermore, an artificial neural network (ANN) approach was used to anticipate the effect of phosphate buffer pH in the activation process on the electrocatalytic activity of the catalyst. This work may open a new gate for the integration of state-of-art electrochemical activation approach to the traditional one and tailoring of noble metal free-alloy electrocatalysts for energy conversion systems.

2. Experimental

2.1. Synthesis of Co_x-Sn_{100-x} alloy nanoparticles

For the Co_x-Sn_{100-x} alloy nanoparticles synthesis, solutions of 0.1 M of cobalt chloride hexahydrate, 0.1 M of tin(II) chloride dihydrate, and 0.2 M of sodium borohydride were prepared. Subsequently, for the synthesis of Co-Sn nanoparticles with different ratios according to Table 1, different amounts of cobalt and tin precursor solutions were transferred into a 200 mL beaker and placed on a magnetic stirrer.

Table 1
Synthesis amounts of different ratios of Co-Sn alloy nanoparticles.

Nanoparticles	Cobalt precursor solution (mL)	Tin precursor solution (mL)	Sodium borohydride solution (mL)	Citric acid (g)
Co_{25}-Sn_{75}	25	75	100	0.44
Co_{35}-Sn_{65}	35	65	100	0.44
Co_{50}-Sn_{50}	50	50	100	0.44
Co_{65}-Sn_{35}	65	35	100	0.44
Co_{75}-Sn_{25}	75	25	100	0.44
Co	100	0	100	0.44
Sn	0	100	100	0.44

Following, 0.44 g of citric acid was introduced to the solution and allowed to be dissolved completely over 10 min. Afterwards, 100 mL of sodium borohydride solution was added drop-wisely to the solution for 15 min. After the addition of sodium borohydride solution, it was allowed to complete the reaction over 15 min. Finally, the resulting solution was centrifuged at 8000 rpm for 10 min and washed with distilled water, and then dried at 80 °C for 4 h [44].

2.2. Characterization of alloy nanoparticles

The structural and morphological features of as-synthesized alloy nanoparticles were explored by means of X-ray diffraction (XRD), field emission scanning electron microscopy (FESEM) with energy-dispersive X-ray spectroscopy (EDX), and transmission electron microscopy (TEM) analysis.

2.3. Preparation of working electrode

To prepare a solution containing a catalyst with a concentration of 1.0 $mg.mL^{-1}$, the catalyst was dispersed in a certain amount of deionized water using an ultrasonic bath. 10 μL of the catalyst ink is drop-casting onto the working electrode, which has already been well polished with alumina slurry. Subsequently, the modified GCE was dried under an IR lamp.

2.4. Electrochemical characterization

The electrochemical characteristics of the modified GCEs with various alloy nanoparticles were investigated by an Autolab type III Potensiostat with a standard three-electrode electrochemical setup consisting of Ag/AgCl, Pt-wire, and nanocatalyst modified-GCE electrode, as the reference electrode, the counter electrode, and the working electrode, respectively. The electrochemical performances of the electrocatalysts were evaluated by cyclic voltammetry (CV), and chronoamperometry (CA) techniques. To begin, CV voltammograms were obtained in 1.0 M NaOH solution at a potential scan rate of 50 $mV.s^{-1}$ to examine the electrochemical properties of the as-synthesized alloy nanoparticles. Moreover, by applying the various anodic potential limits from 0. 7 V to 1.1 V, the metal atoms were allowed to convert to their oxides. Subsequently, CV analysis was carried out at a potential scan rate of 50 $mV.s^{-1}$ in the potential range of −0.3 V to 0.7 V, in 1.0 M methanol and 1.0 M NaOH solution to evaluate the electrocatalytic activity of alloy nanoparticles towards methanol oxidation reaction. Furthermore, as well as the *in-situ* electrochemical activation method, the electrochemical activation approach was conducted by applying various potentials over 300 s in 0.1 M phosphate buffer solution at different pH values ranging between 3 and 12. Moreover, the effect of applied potential during each activation process was investigated at a potential range of −0.7 V to −2.0 V. All of the experiments have been conducted triple times and the average value of them has been presented.

3. Results and discussions

3.1. Physicochemical characterizations of Co_{65}-Sn_{35} alloy nanoparticles

The X-ray diffraction pattern of crystalline material is in the form of thin and sharp peaks; While amorphous materials do not have a clear peak and their X-ray diffraction pattern appears wide. X-ray diffraction pattern of some alloy materials is a mixture of amorphous and crystalline phases. According to part (a) of Fig. 1, Sn nanoparticles have a completely crystalline phase before forming an alloy with Co. According to part (b) of Fig. 1, seven diffraction peaks appeared at angles of 30.89, 32.24, 45.19, 55.74, 62.98, 64.94, and 80.09 degrees, are ascribed to the X-ray reflection from the (200), (101), (211), (301), (112), (400), and (312) planes, respectively, indicating the presence of Sn in the composition [45,46]. Two diffraction at angles of 52.62 and 74.64 degrees related to the X-ray reflection from (200) and (220) planes, respectively, indicate the presence of Co. Also, three diffraction peaks at angles of 29.04, 41.59, and 42.74 degrees reveal the presence of Co-Sn alloy [44,47,48].

To investigate the elemental compositions of the structure of Co_{65}-Sn_{35} alloy nanoparticles, the EDX pattern has been recorded (Fig. 2A). Also, the distribution of elements at high magnification and the profile of changes in the concentration of elements between different areas of the sample have been investigated by qualitative elemental mapping (Fig. 2B). The results of these two analyzes have confirmed the presence of cobalt and tin elements [44,48].

The FESEM image of Co_{65}-Sn_{35} alloy nanoparticles shows the almost spherical as well as irregular morphology of the particles as shown in Fig. 3A and Fig. 3B. Fig. 3A provides general information on the surface area of the alloy nanoparticles and their dispersion, and Fig. 3B shows the particle distribution and almost spherical morphology of the alloy nanoparticles. Determining the average diameter is another piece of information obtained by studying the surface morphology with FESEM. According to Fig. 3C, which shows the size distribution histogram of Co_{65}-Sn_{35} alloy nanoparticles, the average diameter of the synthesized nanoparticles is 42 nm.

Fig. 3D shows the TEM image of Co_{65}-Sn_{35} alloy nanoparticles. Co_{65}-Sn_{35} alloy nanoparticles are almost spherical and no core–shell structure is observed in this image, which confirms that the nanoparticles are alloyed [49]. Alloy formation can also be attributed to the lattice constants of 0.495 and 0.354 nm for Sn and Co, respectively. This small difference in lattice constants, which is smaller than the amplitude of the thermal vibrations of the atoms, can also cause alloying at the nanometer scale [50,51].

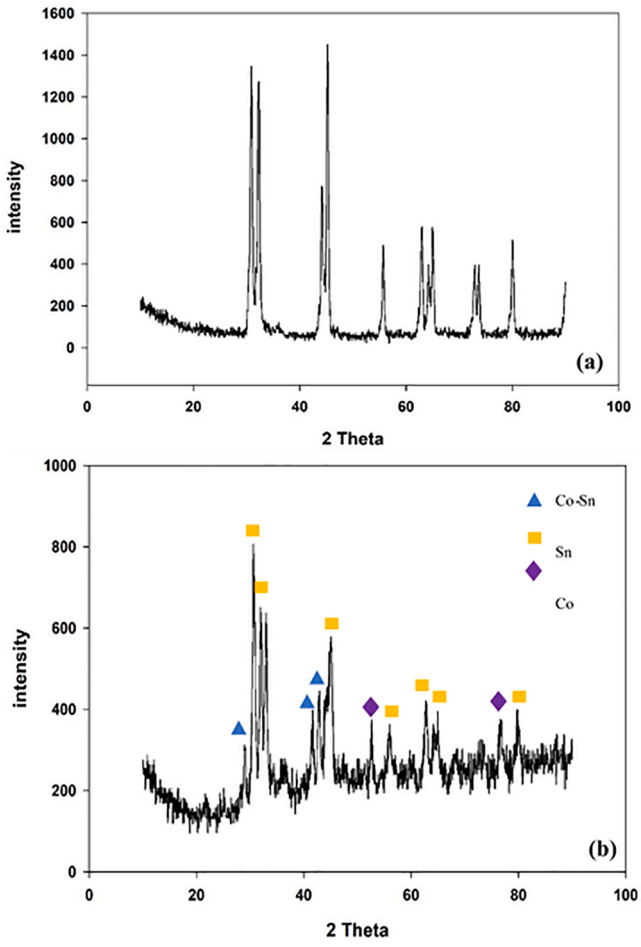

Fig. 1. XRD patterns of (a) Sn nanoparticles and (b) Co_{65}-Sn_{35} alloy nanoparticles.

3.2. Evaluation of electrochemical behavior and optimization studies

Fig. 4A shows the cyclic voltammetry of Co_{65}-Sn_{35} alloy nanoparticles in 1.0 M NaOH solution. In the anodic scan, two identical peaks of A (0.15 V) and B (0.45 V) are attributed to the formation of the oxide layer of Co_{65}-Sn_{35} alloy nanoparticles. In the anodic scan in the region before 0.15 V, the oxidation process of hydrogen atoms adsorbed on the electrode surface takes place. In cathodic scanning, peaks C (0.3 V) and D (zero V) are justified by removing oxide from the surface of the Co_{65}-Sn_{35}/GCE electrode [52].

One of the ways to indicate the formation of metal oxides on the surface of the catalyst is to perform cyclic voltammetry at different limit potentials. Fig. 4B shows the cyclic voltammetry in 1.0 M NaOH solution at limit potentials of 0.7, 0.9, and 1.1 V. By increasing the anodic limit potential from 0.7 to 1.1 V, the peak intensity of the cathodic current increases, which indicates a reduction of metals oxide to metal atoms. On the other hand, the potential of cathode current peaks shifts to more negative values, the reason for this shifting is that, as the threshold potential increases, more metal atoms have the opportunity to convert to metal oxides which are more stable at higher potentials, so more negative potentials in the cathodic scan are required to reduce them.

To investigate the electrocatalytic activity of Co_{65}-Sn_{35} alloy nanoparticles in the methanol oxidation reaction, a cyclic voltammetry technique in the potential range of −0.3 to 0.7 V has been implemented. Fig. 5 shows the cyclic voltammetry curve of Co_{65}-Sn_{35}/GCE electrode in a solution containing 1.0 M methanol and 1.0 M NaOH. The electrocatalytic activity of Co_{65}-Sn_{35} alloy nanoparticles has been compared in three modes including *i)* before activation, *ii)* activation in a phosphate buffer medium, and *iii) in-situ* activation (activation in electrolyte solution). The electrooxidation mechanism of methanol on alloy nanoparticles in alkaline media consists of the following seven steps (here the Co_{65}-Sn_{35} alloy nanoparticles are represented by M). In the first step, the alloy nanoparticles react with methanol in the medium and the methanol is adsorbed on the surface of the alloy nanoparticles (reaction (1)). From the 2nd to the 5th stage, dehydrogenation of methanol molecules is performed (reactions (2) to (5)). In the last two steps, the oxidation–reduction reaction of the alloy nanoparticles is performed and the alloy nanoparticles are returned to medium (reactions (6) and (7)) [53].

$$M + (CH_3OH)_{sol} \leftrightarrow M - (CH_3OH)_{ads} \quad (1)$$

$$M - (CH_3OH)_{ads} + OH^- \leftrightarrow M - (CH_3O)_{ads} + H_2O + e^- \quad (2)$$

$$M - (CH_3O)_{ads} + OH^- \leftrightarrow M - (CH_2O)_{ads} + H_2O + e^- \quad (3)$$

$$M - (CH_2O)_{ads} + OH^- \leftrightarrow M - (CHO)_{ads} + H_2O + e^- \quad (4)$$

$$M - (CHO)_{ads} + OH^- \leftrightarrow M - (CO)_{ads} + H_2O + e^- \quad (5)$$

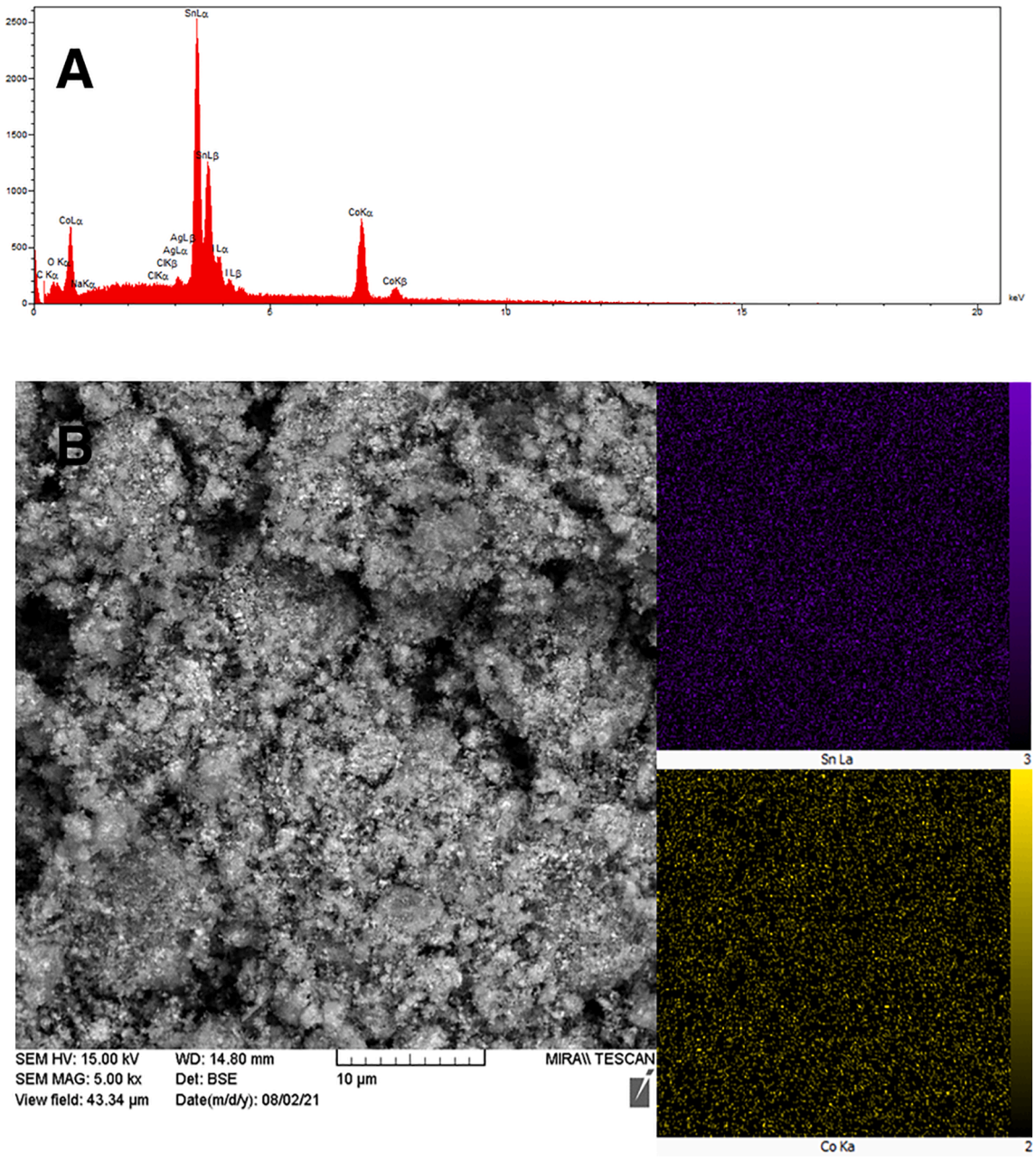

Fig. 2. (A) EDX patterns, (B) Qualitative elemental mapping of Co_{65}-Sn_{35} alloy nanoparticles.

$$M-(CO)_{ads}+OH^{-}\leftrightarrow M-(COOH)_{ads}+e^{-} \quad (6)$$

$$M-(COOH)_{ads}+OH^{-}\leftrightarrow M+CO_2+H_2O+e^{-} \quad (7)$$

According to Fig. 6, the electrocatalytic activity of Co-Sn alloy nanoparticles has been investigated before activation in a solution containing 1.0 M methanol and 1.0 M NaOH. The results have showed that Co_{65}-Sn_{35} alloy has a higher current density and is considered as the optimal alloy nanoparticles. The uniform dispersion of Co_{65}-Sn_{35} alloy nanoparticles and possibly less aggregation and cohesion can be attributed to this [54].

To investigate the effect of phosphate buffer pH in the activation process, the chronoamperometry technique has been employed at a potential of −1.3 V and a fixed time of 300 s. Fig. 7A shows the cyclic voltammetry of Co_{65}-Sn_{35}/GCE electrode in a solution containing 1.0 M methanol and 1.0 M NaOH after activation in phosphate buffer at different pHs. The results have revealed that the highest current density is obtained when the activation process is performed in phosphate buffer with pH = 10. In the activation process with the chronoamperometry technique, a negative potential is implemented, leading to a cathodic reduction reaction at the electrode surface. Fig. 7B shows the cyclic voltammetry of Co_{65}-Sn_{35}/GCE electrode in phosphate buffer solution (pH = 10). In the activation process with phosphate buffer pH = 10, a hydrogen evolution reaction have occured in the range of applied activation potential. The findings have revealed that activation in phosphate buffer solution has led to the formation of more –OH species, thereby boosting the electrocatalytic activation towards MOR in alkaline media.

During the MOR, various parameters affect the electrocatalytic activity of the catalyst. Thereby, especially for large-scale applications, it is crucial to optimize and design this process without conducting redundant experiments. In this context, the ANN method, which is one of the most potent alternatives for modeling both linear and non-linear systems, can be employed both to model and to optimize the process. For future predictions, to model the effect of phosphate buffer pH in the

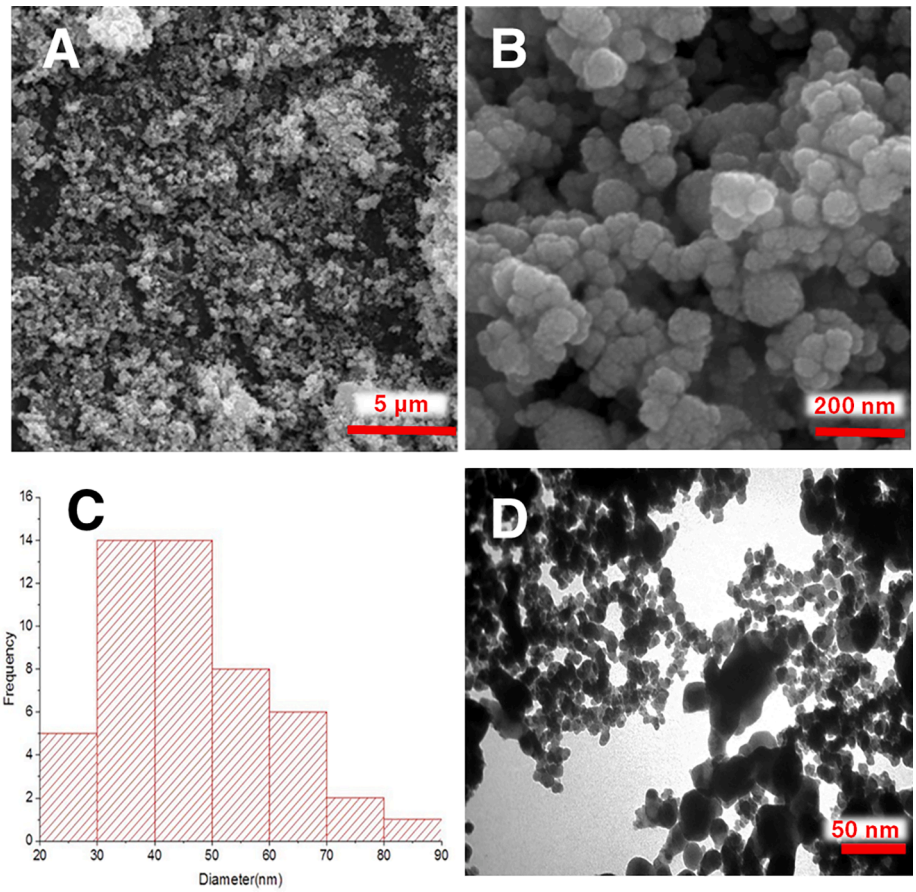

Fig. 3. (A-B) FESEM images (C) Size distribution histogram (D) TEM image of Co_{65}-Sn_{35} alloy nanoparticles.

activation process, the ANN architecture with a hidden layer and 4 neurons in the hidden layer has been implemented. The training algorithm has been selected as Levenberg – Marquardt (LM). The accuracy of the model was confirmed with the values of $R^2 = 0.995$ and RMSE = 0.161. The ANN modeling results have showed that the highest current density for the cyclic voltammetry of Co_{65}-Sn_{35}/GCE electrode has been obtained at pH = 10.05, which is very close to the experimental results. Therefore, it can be concluded that this model will be successfully utilized in future forecasts with high accuracy.

Fig. 8 shows a schematic of the hydrogen evolution reaction in an alkaline medium. According to reaction (8), electrochemical dissociation of water molecules occurs. Then, according to reactions (9) and (10), hydrogen evolution reactions can be performed:

$$H_2O + e^- \rightarrow H^* + OH^- (\text{Volmer}) \quad (8)$$

$$H_2O + H^* + e^- \rightarrow H_2 + OH^- (\text{Heyrovsky}) \quad (9)$$

$$2H^* \rightarrow H_2 (\text{Tafel}) \quad (10)$$

By water dissociation during the activation process, the produced OH species have been adsorbed on the catalyst surface (OH_{ads}) and have boosted the electrocatalytic activity of nanoparticles. According to the results, it is clear that the rate of increase in electrooxidation of methanol in the alkaline medium depends on the Volmer reaction and the better this reaction has taken place. Moreover, the activation process will lead to the production of more OH species on the electrode surface.

To investigate the effect of activation potential in phosphate buffer on methanol electrooxidation, the chronoamperometry technique has been implemented in phosphate buffer solution pH = 10 at different potentials and constant time of 300 s. Fig. 9 shows cyclic voltammetry of Co_{65}-Sn_{35}/GCE electrode in a solution containing 1.0 M methanol and 1.0 M NaOH after activation in phosphate buffer pH = 10. The maximum current density has been achieved when the activation process is performed in phosphate buffer pH = 10 with a potential of −1.3 V. The reason for this can be explained by the difference in the amount of OH_{ads} species produced on the surface of the Co_{65}-Sn_{35}/GCE electrode.

Fig. 10A has showed the cyclic voltammetry of Co_{65}-Sn_{35}/GCE electrode in a solution containing 1.0 M methanol and 1.0 M NaOH after *in-situ* activation process. Since the electrolyte medium is alkaline, the mechanism of the hydrogen evolution reaction in this medium can be used to explain the reason for the increase in current density after activation. The reason for the increase in current after the reduction process at the electrode surface is attributed to the water molecule dissociation, which leads to the production of OH_{ads} species on the electrode surface. Fig. 10B shows the cyclic voltammetry curves of Co_{65}-Sn_{35}/GCE electrode in a solution containing 1.0 M methanol and 1.0 M NaOH after *in-situ* activation at different potentials. The enhanced current density values after *in-situ* activation process have confirmed the boosting effect of the implemented approach. The optimum potential for the activation process to achieve the maximum current density is a potential of −1.3 V.

4. Conclusion

In brief, various Co_x-Sn_{100-x} alloy nanoparticles have been synthesized by facile wet-chemical method and explored as a potential noble-metal free electrocatalyst for alkaline MOR. Physicochemical characterizations have confirmed the successful fabrication of cobalt-tin alloys, with an average nanoparticle diameter of 42 nm. Moreover, the effect of two different electrochemical activation approaches on the electrochemical behavior of the electrocatalyst has been explored. The Co_{65}-Sn_{35} alloy nanoparticles have been determined as the best

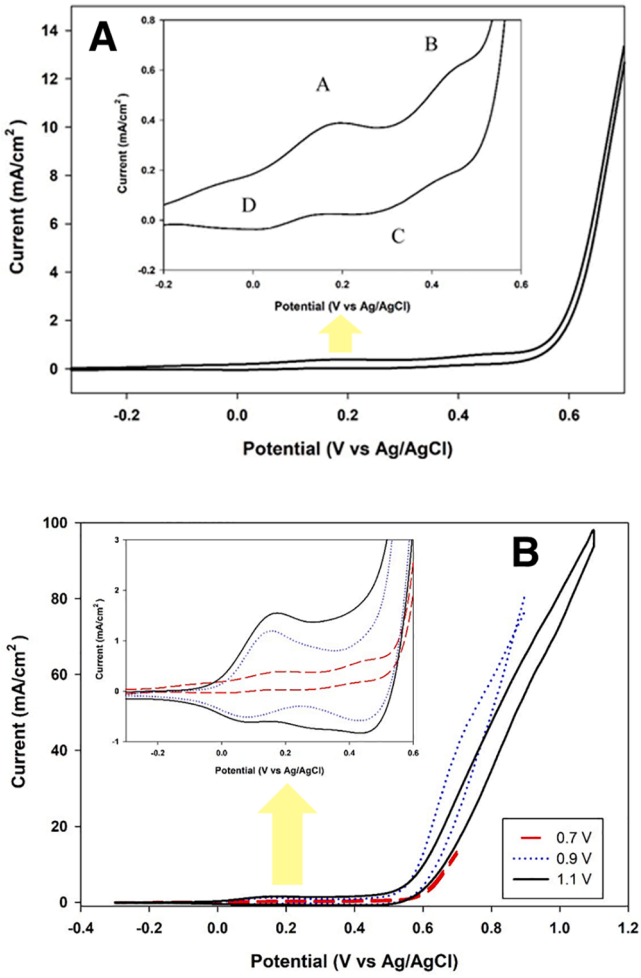

Fig. 4. Cyclic voltammetry of Co_{65}-Sn_{35}/GCE electrode in 1.0 M NaOH solution (A) at the limiting potential of 0.7 V (B) at different limit potentials.

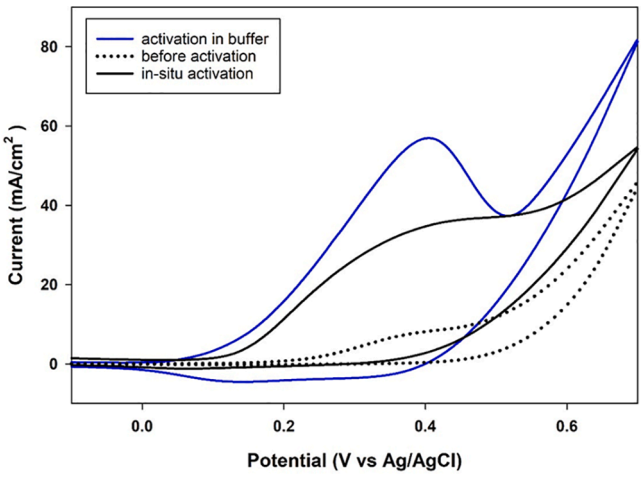

Fig. 5. Cyclic voltammetry curves of Co_{65}-Sn_{35}/GCE electrode in a solution containing 1.0 M methanol and 1.0 M NaOH.

electrocatalyst with the highest current density values, thanks to the uniformly dispersed and less aggregated nanoparticles. Electrochemical in-situ transformation of metal atoms to metal oxides has been carried out using different limit potentials during the cyclic voltammetry experiments to consider the role of metal oxides in boosting

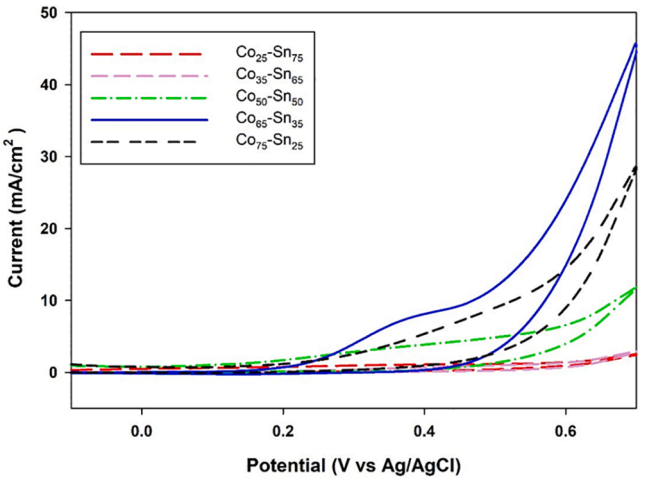

Fig. 6. Cyclic voltammetry of Co-Sn alloy nanoparticles with different ratios in a solution containing 1.0 M methanol and 1.0 M NaOH.

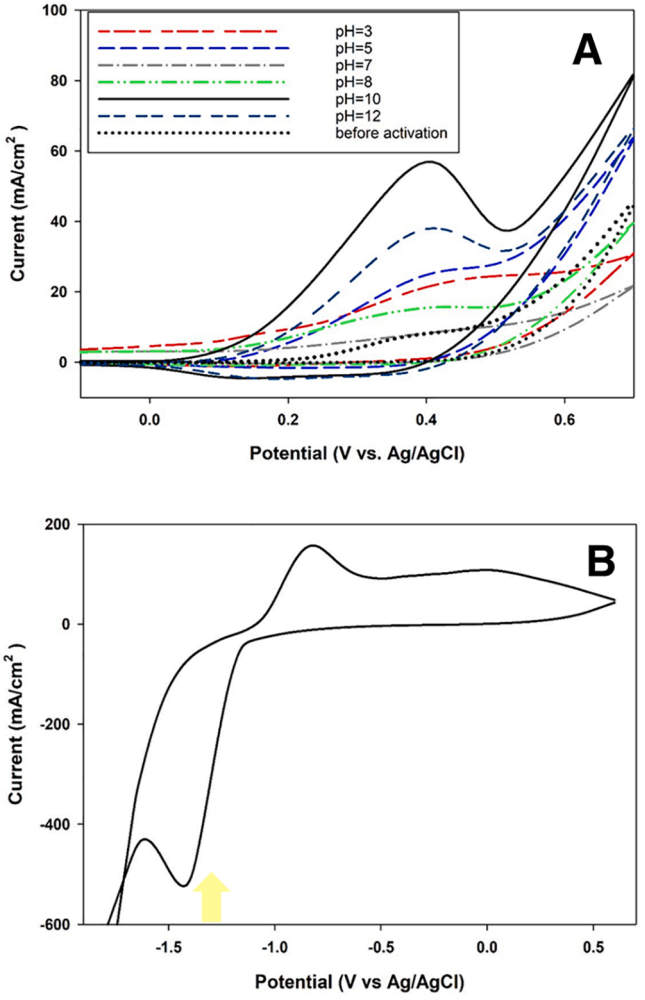

Fig. 7. Cyclic voltammetry curves of Co_{65}-Sn_{35}/GCE electrode in a solution containing 1.0 M methanol and 1.0 M NaOH after activation (A) in phosphate buffer at different pH values ranging between 3 and 12, and (B) in phosphate buffer solution with a pH value of 10.

electrocatalytic performance and facilitating the removal of adsorbed carbon monoxide species on the catalyst surface by providing adsorbed hydroxyl intermediates. Moreover, the electroactivation approach in

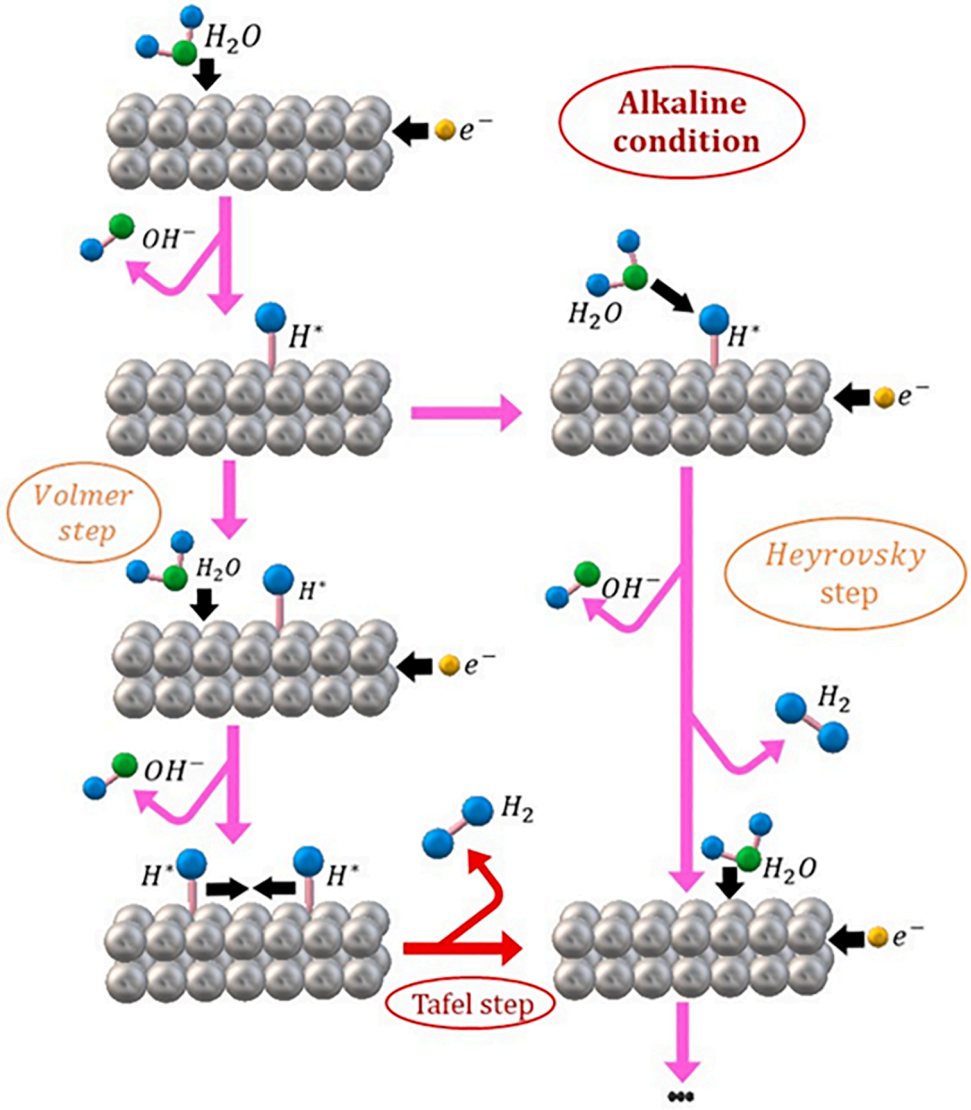

Fig. 8. Schematic presentation of a hydrogen evolution reaction in an alkaline medium.

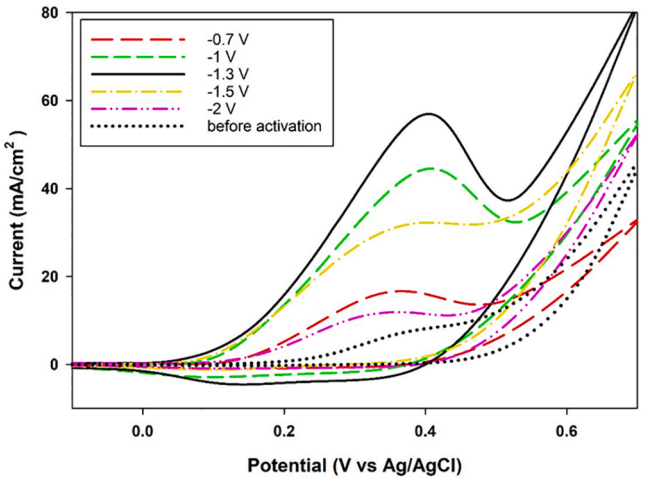

Fig. 9. Cyclic voltammetry curves of Co_{65}-Sn_{35}/GCE electrode in 1.0 M methanol and 1.0 M NaOH solution after activation process in a phosphate buffer solution with a pH value of 10.

phosphate buffer solution with a pH value of 10 was applied by the chronoamperometry method at a constant potential of −1.3 V over a fixed time-period of 300 s. This phenomenon has facilitated the formation of –OH species on the electrode surface, thereby boosting the electrooxidation of methanol in an alkaline medium. Thanks to the *in-situ* activation process, a significant increase in current densities has been observed. This phenomenon was attributed to the fact that the reduction process at the electrode surface leading to the water molecule dissociation, leading to the production of OH_{ads} species on the electrode surface. The proposed activation approaches and straightforward pathway permit the tailoring of the electrochemically active anode electrocatalyst for alkaline MOR to be suitably employed. These revolutionary discoveries potentially lay the ground for the emergence of cutting-edge electrocatalysts based on noble metal-free bimetallic alloy nanoparticles with exceptional performance in fuel cell applications.

CRediT authorship contribution statement

Zeynab Dabirifar: Investigation, Validation, Data curation, Writing – original draft. **Sara Khadempir:** Methodology, Data curation, Investigation, Writing – original draft, Resources. **Alireza Kardan:** Data curation, Investigation, Writing – original draft. **Ceren Karaman:**

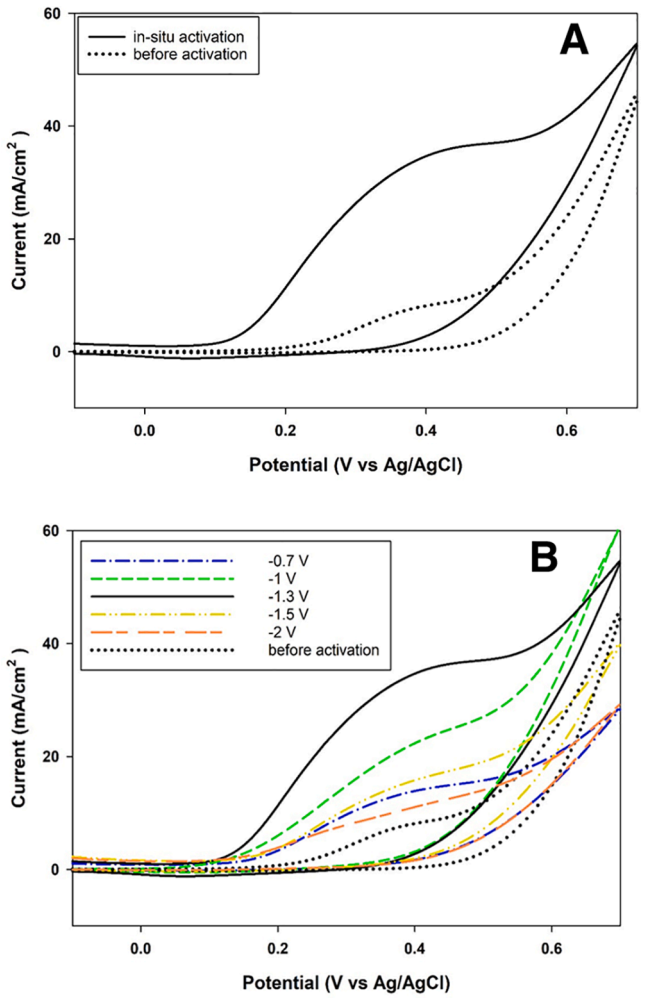

Fig. 10. Cyclic voltammetry curves of Co_{65}-Sn_{35}/GCE electrode in 1.0 M methanol and 1.0 M NaOH solution (A) before and after *in-situ* activation process at a potential of −1.3 V, and (B) after *in-situ* activation process at different potentials ranging between −0.7 to −2.0 V.

Conceptualization, Methodology, Writing – original draft, Writing – review & editing. **Onur Karaman:** Conceptualization, Visualization, Software, Writing – review & editing. **Mehmet Lütfi Yola:** Conceptualization, Writing – review & editing.

Declaration of Competing Interest

The authors declare that they have no known competing financial interests or personal relationships that could have appeared to influence the work reported in this paper.

References

[1] Acar C, Dincer I. Review and evaluation of hydrogen production options for better environment. J Clean Prod 2019;218:835–49.
[2] Acar C, Dincer I, Naterer GF. Review of photocatalytic water-splitting methods for sustainable hydrogen production. Int J Energ Res 2016;40(11):1449–73.
[3] Taherian Z, Shahed Gharahshiran V, Khataee A, Orooji Y. Synergistic effect of freeze-drying and promoters on the catalytic performance of Ni/MgAl layered double hydroxide. 2022; 311: 122620.
[4] Dincer I, Acar C. Review and evaluation of hydrogen production methods for better sustainability. Int J Hydrogen Energ 2015;40(34):11094–111.
[5] Dincer I, Rosen MA. Sustainability aspects of hydrogen and fuel cell systems. Energy Sustain Dev 2011;15(2):137–46.
[6] Dincer I, Zamfirescu C. Sustainable Hydrogen Production. Sustain Hydrogen Product 2016:1–479.
[7] Taherian Z, Khataee A, Han N, Orooji Y. Hydrogen production through methane reforming processes using promoted-Ni/mesoporous silica: A review. J Ind Eng Chem 2022;107:20–30.
[8] Ozoemena KI. Nanostructured platinum-free electrocatalysts in alkaline direct alcohol fuel cells: catalyst design, principles and applications. Rsc Adv 2016;6(92):89523–50.
[9] Zhang J, Lu SF, Xiang Y, Shen PK, Liu J, Jiang SP. Carbon-Nanotubes-Supported Pd Nanoparticles for Alcohol Oxidations in Fuel Cells: Effect of Number of Nanotube Walls on Activity. ChemSusChem 2015;8(17):2956–66.
[10] Glusen A, Dionigi F, Paciok P, Heggen M, Muller M, Gan L, et al. Dealloyed PtNi-Core-Shell Nanocatalysts Enable Significant Lowering of Pt Electrode Content in Direct Methanol Fuel Cells. Acs Catal 2019;9(5):3764–72.
[11] Gu ZL, Xu H, Bin D, Yan B, Li SM, Xiong ZP, et al. Preparation of PdNi nanospheres with enhanced catalytic performance for methanol electrooxidation in alkaline medium. Colloid Surface A 2017;529:651–8.
[12] Zhao X, Yin M, Ma L, Liang L, Liu CP, Liao JH, et al. Recent advances in catalysts for direct methanol fuel cells. Energ Environ Sci 2011;4(8):2736–53.
[13] Dasdelen Z, Yildiz Y, Eris S, Sen F. Enhanced electrocatalytic activity and durability of Pt nanoparticles decorated on GO-PVP hybride material for methanol oxidation reaction. Appl Catal B-Environ 2017;219:511–6.
[14] Hu TJ, Wang Y, Liu Q, Zhang LN, Wang HB, Tang T, et al. In-situ synthesis of palladium-base binary metal oxide nanoparticles with enhanced electrocatalytic activity for ethylene glycol and glycerol oxidation. Int J Hydrogen Energ 2017;42(41):25951–9.
[15] Arefi-Oskoui S, Khataee A, Behrouz SJ, Vatanpour V, Gharamaleki SH, Orooji Y, et al. Development of MoS2/O-MWCNTs/PES blended membrane for efficient removal of dyes, antibiotic, and protein. Sep Purif Technol 2022;280:119822.
[16] Keyikoglu R, Khataee A, Lin H, Orooji Y. Vanadium (V)-doped ZnFe LDH for enhanced sonocatalytic degradation of pymetrozine. Chem Eng J 2022;434:134730.
[17] Karimi-Maleh H, Cellat K, Arikan K, Savk A, Karimi F, Sen F. Palladium-Nickel nanoparticles decorated on Functionalized-MWCNT for high precision non-enzymatic glucose sensing. Mater Chem Phys 2020;250.
[18] Karimi-Maleh H, Mousavi SJ, Mahdavian M, Khaleghi M, Bordbar S, Yola ML, et al. Effects of silver nanoparticles added into polyurea coating on sulfate-reducing bacteria activity and electrochemical properties; an environmental nano-biotechnology investigation. Environ Res 2021;198.
[19] Qian H, Wang J, Yan L. Synthesis of Lignin-Poly(N-methylaniline)-Reduced Graphene Oxide Hydrogel for Organic Dye and Lead Ions Removal. J Bioresour Bioprod 2020;5(3):204–10.
[20] Zhang H, Jiang J, Li J, Li Y, Zhou L, Gao H, et al. Preparation and properties of TiO2/chitosan/acrylic acid in situ cross-linked composite hydrogel. J Forest Eng 2020;5:76–81.
[21] Deeksha B, Sadanand V, Hariram N, Rajulu AV. Preparation and properties of cellulose nanocomposite fabrics with in situ generated silver nanoparticles by bioreduction method. J Bioresour Bioprod 2021;6(1):75–81.
[22] Al Sharabati M, Abokwiek R, Al-Othman A, Tawalbeh M, Karaman C, Orooji Y, et al. Biodegradable polymers and their nano-composites for the removal of endocrine-disrupting chemicals (EDCs) from wastewater: a review. Environ Res 2021;202.
[23] Joseph B, Sagarika VK, Sabu C, Kalarikkal N, Thomas S. Cellulose nanocomposites: fabrication and biomedical applications. J Bioresour Bioprod 2020;5(4):223–37.
[24] Sohrabi H, Majidi MR, Arbabzadeh O, Khaaki P, Pourmohammad S, Khataee A, et al. Recent advances in the highly sensitive determination of zearalenone residues in water and environmental resources with electrochemical biosensors. Environ Res 2022;204.
[25] Zhang Y, Wei L, Lu L, Gan L, Mingzhu P. Adsorption-photocatalytic properties of cellulose nanocrystal supported ZnO nanocomposites. journal of Forestry. Engineering 2020;5:29–35.
[26] Karaman C, Karaman O, Show PL, Karimi-Maleh H, Zare N. Congo red dye removal from aqueous environment by cationic surfactant modified-biomass derived carbon: Equilibrium, kinetic, and thermodynamic modeling, and forecasting via artificial neural network approach. Chemosphere 2021;133346.
[27] Karaman C, Karaman O, Show PL, Orooji Y, Karimi-Maleh H. Utilization of a double-cross-linked amino-functionalized three-dimensional graphene networks as a monolithic adsorbent for methyl orange removal: equilibrium, kinetics, thermodynamics and artificial neural network modeling. Environ Res 2021;112156.
[28] Hyder A, Buledi JA, Nawaz M, Rajpar DB, Shah ZUH, Orooji Y, et al. Identification of heavy metal ions from aqueous environment through gold, Silver and Copper Nanoparticles: An excellent colorimetric approach. Environ Res 2022; 205.
[29] Karaman O. Oxygen Reduction Reaction Performance Boosting Effect of Nitrogen/Sulfur Co-Doped Graphene Supported Cobalt Phosphide Nanoelectrocatalyst: pH-Universal Electrocatalyst. Ecs J Solid State Sc 2021;10(6).
[30] Karaman C, Karaman O, Atar N, Yola ML. Sustainable electrode material for high-energy supercapacitor: biomass-derived graphene-like porous carbon with three-dimensional hierarchically ordered ion highways. Phys Chem Chem Phys 2021;23(22):12807–21.
[31] Karimi-Maleh H, Karimi F, Fu L, Sanati AL, Alizadeh M, Karaman C, et al. Cyanazine herbicide monitoring as a hazardous substance by a DNA nanostructure biosensor. J Hazard Mater 2022;423.
[32] Karimi-Maleh H, Khataee A, Karimi F, Baghayeri M, Fu L, Rouhi J, et al. A green and sensitive guanine-based DNA biosensor for idarubicin anticancer monitoring in biological samples: A simple and fast strategy for control of health quality in chemotherapy procedure confirmed by docking investigation. Chemosphere 2021;132928.

[33] Cheraghi S, Taher MA, Karimi-Maleh H, Karimi F, Shabani-Nooshabadi M, Alizadeh M, et al. Novel enzymatic graphene oxide based biosensor for the detection of glutathione in biological body fluids. Chemosphere 2022;287.
[34] Roostaee M, Sheikhshoaei I, Karimi-Maleh H. Fe3O4@Au-rGO Nanocomposite/Ionic Liquid Modified Sensor for Ultrasensitive and Selective Sensing of Doxorubicin. Top Catal 2022.
[35] Cheng Z, Meng J, Wang X. Preparation of wood-based filter loaded with Ag nanoparticles and its catalytic degradation performance on organic dye. J Forest Eng 2020;50(6):94–8.
[36] Karaman C. Orange Peel Derived-Nitrogen and Sulfur Co-doped Carbon Dots: a Nano-booster for Enhancing ORR Electrocatalytic Performance of 3D Graphene Networks. Electroanal 2021;33(5):1356–69.
[37] Karaman C, Karaman O, Atar N, Yola ML. Tailoring of cobalt phosphide anchored nitrogen and sulfur co-doped three dimensional graphene hybrid: Boosted electrocatalytic performance towards hydrogen evolution reaction. Electrochim Acta 2021;380.
[38] Ingavale SB, Patil I, Parse H, Sesu DC, Marbaniang P, Ramgir N, et al. Polyoxomolybdate anchored graphite oxide: Noble metal-free electrocatalyst for oxygen reduction reaction. Int J Hydrogen Energ 2019;44(45):24922–33.
[39] Ke FS, Huang L, Cai JS, Sun SG. Electroplating synthesis and electrochemical properties of macroporous Sn-Cu alloy electrode for lithium-ion batteries. Electrochim Acta 2007;52(24):6741–7.
[40] Yang CG, Zhang DW, Zhao YB, Lu YH, Wang L, Goodenough JB. Nickel foam supported Sn-Co alloy film as anode for lithium ion batteries. J Power Sources 2011;196(24):10673–8.
[41] Wang Z, Tian WH, Liu XH, Yang R, Li XG. Synthesis and electrochemical performances of amorphous carbon-coated Sn-Sb particles as anode material for lithium-ion batteries. J Solid State Chem 2007;180(12):3360–5.
[42] Hayden BE, Rendall ME, South O. Electro-oxidation of carbon monoxide on well-ordered pt(111)/Sn surface alloys. J Am Chem Soc 2003;125(25):7738–42.
[43] Jang BO, Park SH, Lee WJ. Electrospun Co-Sn alloy/carbon nanofibers composite anode for lithium ion batteries. J Alloy Compd 2013;574:325–30.
[44] Milanova V, Atanasova S, Avdeev G, Markova I. Morphology of intermetallic (Co-Sn, Ni-Sn) nanoparticles, electrochemicaly tested as electrodes in li-ion battery. J Chem Technol Metall 2017;52(3):542–56.
[45] Wu P, Du N, Zhang H, Yu JX, Qi Y, Yang DR. Carbon-coated SnO2 nanotubes: template-engaged synthesis and their application in lithium-ion batteries. Nanoscale 2011;3(2):746–50.
[46] Zhang J, Ma ZS, Jiang WJ, Zou YL, Wang Y, Lu CS. Sandwich-like CNTs@SnO2/SnO/Sn anodes on three-dimensional Ni foam substrate for lithium ion batteries. J Electroanal Chem 2016;767:49–55.
[47] Milanova V, Markova I, Piskin M, Stankulov T, Petrov T, Denev I. Synthesis and study of carbon-based nanocomposites with Co-Sn nanoparticles for electrode materials. J Chem Technol Metall 2015;50(3):288–98.
[48] Khe C, Aziz A, Lockman Z. Synthesis of Cobalt/Gold Bimetallic Particles with Porous Flake-Like Nanostructures and Their Magnetic Properties. Nanosci Nanotech Let 2012;4(7):687–92.
[49] Yang MM, Wang ZY, Wang W, Liu CJ. Synthesis of AuPd alloyed nanoparticles via room-temperature electron reduction with argon glow discharge as electron source. Nanoscale Res Lett 2014;9.
[50] Mailu SN, Waryo TT, Ndangili PM, Ngece FR, Baleg AA, Baker PG, et al. Determination of Anthracene on Ag-Au Alloy Nanoparticles/Overoxidized-Polypyrrole Composite Modified Glassy Carbon Electrodes. Sensors-Basel 2010;10(10):9449–65.
[51] Betteridge W. The properties of metallic cobalt. Prog Mater Sci 1980;24:51–142.
[52] Hassan KM, Hathoot AA, Maher R, Azzem MA. Electrocatalytic oxidation of ethanol at Pd, Pt, Pd/Pt and Pt/Pd nano particles supported on poly 1,8-diaminonaphthalene film in alkaline medium. Rsc Adv 2018;8(28):15417–26.
[53] Song YY, Zhang XL, Yang S, Wei X, Sun ZB. Electrocatalytic performance for methanol oxidation on nanoporous Pd/NiO composites prepared by one-step dealloying. Fuel 2016;181:269–76.
[54] Ghouri ZK, Barakat NAM, Kim HY. Influence of copper content on the electrocatalytic activity toward methanol oxidation of Co chi Cuy alloy nanoparticles-decorated CNFs. Sci Rep-Uk 2015;5.